Astron. Astrophys. 357, 767–776 (2000)

ASTRONOMY AND ASTROPHYSICS

A study of opacity in SOHO-SUMER and SOHO-CDS spectral observations

II. Atmospheric structure at the solar limb

G.A. Fischbacher, S.D. Loch, and H.P. Summers

University of Strathclyde, 107 Rottenrow, Glasgow G4 0NG, UK

Received 31 December 1999 / Accepted 20 January 2000

Abstract. To model the EUV emission from solar plasma at transition region temperatures it is necessary to take account of both the structure and dynamics of the plasma and the effects of opacity which radiatively couple different points within the plasma. Simple escape probability techniques exist which avoid the need for a full solution of the radiative transfer equation. These have been used to diagnose spectral line opacities, to calculate excited state population structures and have also been used in conjunction with simple atmosphere models to calculate limb brightening curves and the variation of selected line ratios on crossing the limb.

In this work we firstly revisit these techniques and extend them for use with some stratified atmosphere models. The objective is to assess the continuing effectiveness of such methods within more detailed structural and dynamic atmosphere pictures. We find that although the emission characteristics are dominated by inhomogeneities, the observed opacities are less sensitive and may be reasonably well accounted for within a stratified atmosphere model.

Secondly, we develop the escape probability techniques to examine modifications to the population structure and line blending, and use them in conjunction with the stratified atmosphere models to predict both limb brightening and the variation of branching multiplet ratios on crossing the limb. Results are compared with observations by the SUMER instrument on board the SOHO spacecraft.

Key words: radiative transfer – Sun: atmosphere – Sun: transition region – Sun: UV radiation

1. Introduction

The effects of opacity in solar spectral lines have been studied on a number of occasions (Jordan 1967; Doschek et al. 1976; Doyle & McWhirter 1980). Jordan (1967) established the technique of using branching ratios of lines arising from a common upper level to extract information on opacities from spectral observations. Doyle & McWhirter subsequently developed this same technique to study opacity at the solar limb and their work included a simple model of predicted line ratios from the region on-disk up to the limb. Escape probability and escape factor expressions originated with the work of Holstein, 1947 (see also McWhirter 1965; Irons 1979). More recently Kastner & Kastner (1990), Kastner & Bhatia (1989) and Kastner & Bhatia (1992) have reworked escape probability expressions and have used them for predicting emergent intensities and optically thick population structures. The latter paper contained predicted limb brightening curves and ratio variations for a number of C III lines.

In paper I of this series (Brooks et al. 2000) the observational approach of Doyle & McWhirter was extended and used in an analysis of spectral data from the SOHO spectrometers CDS and SUMER with three objectives in mind: firstly to present some systematics of the incidence of opacity along iso-electronic sequences; secondly to extend the Doyle & McWhirter analysis to the case of lines with optical thicknesses significantly greater than unity on the solar disk and thirdly to judge the suitability of lines observed by CDS and SUMER for differential emission measure analysis (DEM).

In the present paper this approach is developed further in order to assess the escape probability as a modelling tool within dynamic and detailed structural atmospheric models. The escape probability approach for dealing with opacity has the advantage that it is relatively simple, avoiding the need for a full solution of the radiative transfer equation. Since the chromosphere and transition-zone represent regions of non-negligible opacity from which the spectral emission is dominated by atmospheric structure, such techniques are potentially very useful. The theory is developed to include consistent modification to the population structure within the atmosphere models considered and the effects of line blending on the emergent intensities and population structure. We seek also to take better account of the geometric extension of the line of sight at the limb to predict both limb brightening and branching ratio variations on crossing the limb for selected lines of C II and C III. As in paper I these predictions are compared with observational data from SUMER. In paper I it was shown that off-limb the branching ratio characteristics are dominated by the presence of instru-

Send offprint requests to: G.A. Fischbacher

mentally scattered light. This effect is also accounted for within the new models.

2. Theory

The spectral emission from a plasma is governed by two sets of coupled equations, namely the radiative transfer equations and the equations of statistical balance. These may be written as (McWhirter 1965)

$$\frac{dI_\nu}{dl} = j_\nu - \kappa_\nu I_\nu \tag{1}$$

$$\frac{dN_u}{dt} = -A_{u\to l}N_u + B_{u\to l}N_l \int_0^\infty \bar{I}_\nu \phi(\nu) d\nu + \textit{other collisional and radiative terms} \tag{2}$$

Here I_ν is the photon intensity; dl is an element of distance along the line of sight; $\phi(\nu)$ is the line profile (emission and absorption profiles are assumed here to be equal); j_ν is the photon emissivity – the number of photons emitted/unit time/unit volume/unit solid angle – which, if stimulated emission is ignored, is given by

$$j_\nu = \frac{1}{4\pi} A_{u\to l} N_u \phi(\nu) \tag{3}$$

where $A_{u\to l}$ is the Einstein A-coefficient. κ_ν is the absorption coefficient which is defined such that $\kappa_\nu I_\nu$ is the number of photons absorbed/unit time/unit volume/unit solid angle. κ_ν is therefore given by

$$\kappa_\nu = \frac{1}{c} N_l h\nu B_{l\to u} \phi(\nu) \tag{4}$$

where $B_{l\to u}$ is the Einstein B-coefficient. Finally, N_u and N_l are the upper and lower level population densities respectively and $\bar{I}_\nu$ is the intensity averaged over direction. Note that Eq. 2 is equivalent to Eq. 1 of Bhatia & Kastner (1992).

Using the relation between the Einstein A and B-coefficients, Eqs. 1 and 2 become

$$\frac{dI(\mathbf{x},\mathbf{r})}{dl} = \frac{1}{4\pi} A_{u\to l} N_u(\mathbf{r}) \left[1 - \frac{N_l(\mathbf{r})\omega_u}{N_u(\mathbf{r})\omega_l} \frac{c^2}{2\nu_0^2} \times \int I_\nu(\mathbf{x},\mathbf{r}) \phi(\nu) d\nu \right] \tag{5}$$

$$\frac{dN_u(\mathbf{r})}{dt} = -A_{u\to l} N_u(\mathbf{r}) \left[1 - \frac{N_l(\mathbf{r})\omega_u}{N_u(\mathbf{r})\omega_l} \frac{c^2}{2\nu_0^2} \times \int \bar{I}_\nu(\mathbf{r}) \phi(\nu) d\nu \right] + \textit{other collisional and radiative terms} \tag{6}$$

where the spatial dependances have been put in explicitly.

The terms in the brackets are markedly similar, the only difference being in the specification of the intensity terms. In the radiative transfer case the intensity term $I_\nu(\mathbf{x},\mathbf{r})$ is the intensity at the point $\mathbf{r}$ due to the source $\mathbf{x}$ and so is related to the emissivity, j_ν, along the path $\mathbf{x} \to \mathbf{r}$. In the population case, however, $\bar{I}_\nu(\mathbf{r})$ is the radiation field at $\mathbf{r}$ due to the surrounding plasma and so is related to the integral of $j_\nu(\mathbf{x})$, and thus the integral of $N_u(\mathbf{x})$, over all points $\mathbf{x}$.

Eqs. 5 and 6 can be re-written as follows:

$$\frac{dI}{dl} = \frac{1}{4\pi} A_{u\to l} N_u(\mathbf{r}) g\{\tau_0(\mathbf{x},\mathbf{r})\} \tag{7}$$

$$\frac{dN_u(\mathbf{r})}{dt} = -A_{u\to l} N_u(\mathbf{r}) \Lambda(\mathbf{r}) + \textit{the other terms} \tag{8}$$

$g\{\tau_0(\mathbf{x},\mathbf{r})\}$ is called the *escape probability* which represents the probability that a photon will propagate a distance $|\mathbf{r}-\mathbf{x}|$ along the path $\mathbf{x} \to \mathbf{r}$ without being absorbed. $\tau_0(\mathbf{x},\mathbf{r})$ is the optical depth at line centre defined by

$$\tau_0(\mathbf{x},\mathbf{r}) = \tilde{\kappa}_0 \int_{\mathbf{x}\to\mathbf{r}} N_l(\mathbf{r}') dl \tag{9}$$

with

$$\tilde{\kappa}_0 = \frac{\kappa_\nu}{N_l \phi(\nu)} \tag{10}$$

g is identical to what Irons (1979) calls the transmission coefficient but is called here the escape probability since the point $\mathbf{r}$ is outwith the emitting plasma. $\Lambda(\mathbf{r})$ is called the Biberman-Holstein coefficient (hereafter referred to as the *absorption factor*) which represents 1 - the probability that a net absorption will occur at the point $\mathbf{r}$. These quantities act to parametrically adjust the Einstien A-coefficients in the optically thin radiative transfer and statistical balance equations to account for the effects of self-absorption.

2.1. The escape probability

The escape probability, as introduced by Holstein (1947), has subsequently been considered by many authors (eg. McWhirter 1965; Irons 1979; Kastner & Kastner 1990). Holstein showed that assuming a constant source function and that spectral lines are purely doppler broadened, the escape probability may be written as

$$g\{\tau_0(\mathbf{x},\mathbf{r})\} = \frac{1}{\sqrt{\pi}} \int_{-\infty}^{\infty} e^{-u^2}\, exp\{-\tau_0(\mathbf{x},\mathbf{r}) e^{-u^2}\}\, du \tag{11}$$

From Eq. 7 the solution of the equation of radiative transfer may be written as

$$I = \frac{1}{4\pi} A_{u\to l} \int_{l.o.s.} N_u(\mathbf{r}) g\{\tau_0(\mathbf{x},\mathbf{r})\} dl \tag{12}$$

where $\mathbf{x}$ corresponds to a position outwith the layer. Making the further assumption that N_u is constant we obtain

$$I = \frac{1}{4\pi} A_{u\to l} N_u \bar{g}\{\tau_0\} \Delta x \tag{13}$$

where Δx is the thickness of the emitting layer. $\bar{g}\{\tau_0\}$ represents the mean probability that a line photon emitted somewhere along the line of sight in the direction of the observer will escape

along the line of sight without being absorbed. τ_0 is the total optical depth of the layer along the line of sight. It was shown by Kastner & Kastner (1990) that this quantity, which they term $p_f(\hat{\nu}, \vec{k}, \tau : 1)$, is given by

$$\bar{g}\{\tau_0\} \equiv p_f(\hat{\nu}, \vec{k}, \tau : 1) = \frac{1}{\sqrt{\pi}} \int_{-\infty}^{\infty} \left\{ \frac{1 - exp[-\tau_0 e^{-x^2}]}{\tau_0} \right\} dx \quad (14)$$

From this follows a simple idea, which was introduced by Jordan (1967), for extracting optical depth from observations of intensity ratios of spectral lines arising from a common upper level. Such ratios may be written as

$$\frac{I_{u\rightarrow l_1}}{I_{u\rightarrow l_2}} = \frac{A_{u\rightarrow l_1}}{A_{u\rightarrow l_2}} \frac{\bar{g}\{\tau_{0,l_1\rightarrow u}\}}{\bar{g}\{\tau_{0,l_2\rightarrow u}\}} \quad (15)$$

In optically thin conditions this ratio reduces to that of the Einstein A-coefficients and opacity is the only mechanism that can modify it from this value. The transitions that are most significantly affected are those with large and long lived lower level populations – i.e. metastables. However, such populations are themselves not significantly modified due to their large value and are collisionally controlled. Thus the ratio of optical depths of two optically thick lines arising from a common upper level is constant – i.e.

$$\tau_{0,l_2\rightarrow u} = \frac{N_{l_2} f_{l_2\rightarrow u}}{N_{l_1} f_{l_1\rightarrow u}} \times \tau_{0,l_1\rightarrow u} = c \times \tau_{0,l_1\rightarrow u} \quad (16)$$

where $f_{l_1\rightarrow u}$ and $f_{l_2\rightarrow u}$ are oscillator strengths. Since c is a constant, Eq. 15 may be written as

$$\frac{I_{u\rightarrow l_1}}{I_{u\rightarrow l_2}} = \frac{A_{u\rightarrow l_1}}{A_{u\rightarrow l_2}} \frac{\bar{g}\{\tau_{0,l_1\rightarrow u}\}}{\bar{g}\{c \times \tau_{0,l_1\rightarrow u}\}} \quad (17)$$

This equation provides the route for extracting optical depth from observations. Once the optical depth is known for one line, those of all the other lines of the same ion whose lower levels are metastable can be obtained via Eq. 16. Assuming the other lines of the same ion (those whose lower levels are not metastable) are optically thin, the opacities of all the lines of an ion can be obtained from the single extracted value. In paper I this analysis was performed for lines of C II and C III using SUMER data to assess which lines should be rejected or intensity adjusted in a DEM analysis.

2.2. Absorption factors

The two principle effects of opacity are

1. Loss of photons out of the line of sight
2. Modification to the population structure due to photo-absorptions

The absorption of a photon by an atom or ion results in an electron excitation which can lead to either a re-emission of a photon in the reverse process or a collisional de-excitation. It is conventional within radiative transfer theory to distinguish between these two cases since the former (scattering) leads to no thermal coupling between the emitting and the absorbing plasma, whereas the latter case (pure absorption) does. Furthermore this distinction is useful in dealing with a third effect of opacity, namely partial frequency redistribution in which the emission profiles are modified due to scattering.

This distinction is not always so clear in escape probability literature. However, as described above, it influences the populations and emergent intensities via the effect of partial frequency redistribution and as yet this effect has not been included within an escape probability model.

The escape probability takes account of the loss of photons out of the line of sight due to both scattering and absorption. However, this quantity is not sufficient in describing the effects of opacity on spectral emission. Along the line of sight photons are absorbed from all directions leading to an enhanced upper level population and consequently an increase in emission in the line of sight. This is described by some authors as scattering into the line of sight (e.g. Kastner & Bhatia 1992).

In essence Kastner & Bhatia formulate the problem as follows:

$$I^{(o.thick)} \sim \int_{l.o.s.} N_u^{(o.thin)}(\mathbf{r}) A_{u\rightarrow l}^{(o.thick)} g\{\tau_0(\mathbf{x}, \mathbf{r})\} dl \quad (18)$$

where '$l.o.s.$' denotes line-of-sight. Jordan (1967) wrote that the energy emissivity, E, of line *i* can be expressed as

$$E_i \sim N_u W_i = \frac{N_u b_i q_i}{1 - \sum_n (b_n[1 - q_n])} \quad (19)$$

where q_i the probability of escape (equivalent in principle to $\bar{g}\{\tau_{0,i}\}$) and b_i the probability that a photon will be emitted in line i. W_i was re-evaluated by Kastner & Bhatia (1992) as

$$b_i p_{e,j} = \frac{b_i \vec{p}_{f,j}}{1 - \sum_i b_i (1 - p_{d,i})(1 - \bar{p}_{f,i})(1 - \vec{p}_{f,i})} \quad (20)$$

where $p_{d,i}$ is the photon loss probability, $\vec{p}_{f,j} = p_f(\hat{\nu}, \vec{k}, \tau : 1) \equiv \bar{g}\{\tau_0\}$, and $\bar{p}_{f,i} = p_f(\hat{\nu}, \hat{\vec{k}}, \tau : 0)$ is the mean probability that a photon emitted anywhere in the layer will travel to the surface and escape. This latter term is equivalent to Irons' escape factor, θ (Irons 1979). $A_{u\rightarrow l}^{(o.thick)}$ is given by $A_{u\rightarrow l}^{(o.thin)}$ divided by the denominator of $p_{e,j}$.

Jordan noted that in the case of intensity ratios of lines arising from a common upper level the denominator cancels and thus the population modification does not influence these ratios.

The problem with this approach is that it does not take full account of the indirect effects on the population structure. In the formulation of Eq. 19, Jordan considered emission in line *i* from a point to be characterised by an optically thin population structure. She then considered the ultimate fate of those emitted photons allowing them to be absorbed in line *i*, subsequently re-emitted in any line stemming from the same upper level, subsequently re-absorbed again, and so on and so forth.

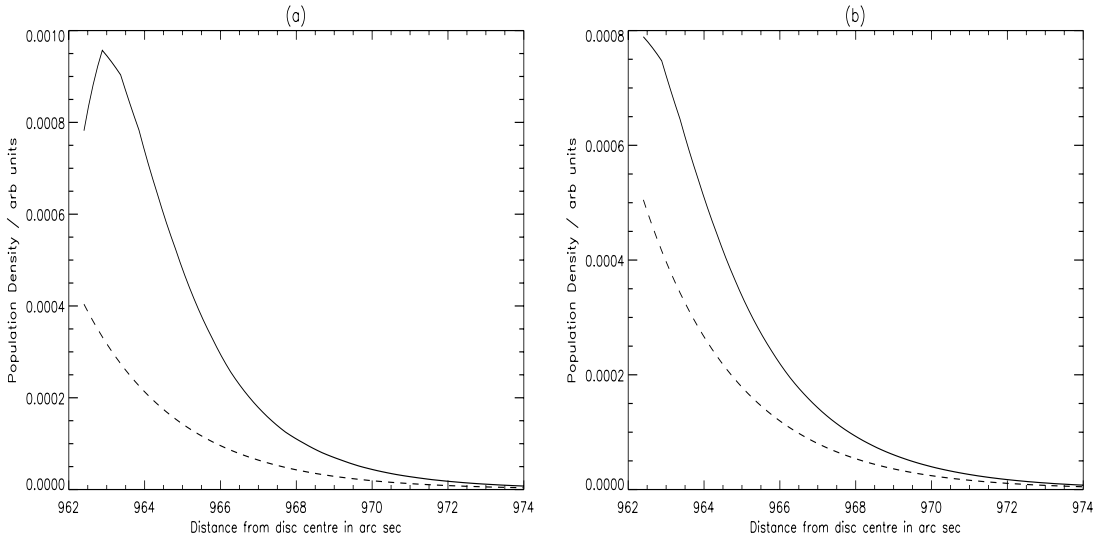

Fig. 1. **a** Optically thin (dashed line) and thick (solid line) population density distributions for model 3 (see Sect. 3) for the C II $2s^2 2p\ ^2P_{3/2} - 2s2p^2\ ^2P_{3/2}$ line at 904.143 Å for an optical depth of 4. **b** Optically thin (dashed line) and thick (solid line) population density distributions for model 3 for the C II $2s^2 2p\ ^2P_{3/2} - 2s2p^2\ ^2S_{1/2}$ line at 1037.020 Å for an optical depth of 1.46 which corresponds to the same circumstances as in **a**. In contrast to **a** the modified population distribution in **b** is closely approximated by a constant $\times$ the optically thin distribution.

However, this does not take account of the contribution to line *i* of photons initially emitted in lines other than *i*, but from the same upper level, that are re-absorbed leading to emission in line *i*. This contribution is of particular importance for lines that are relatively thin if there exist thick lines stemming from the same upper level.

In addition if there is some line blending then photons emitted in one line in the blend may be absorbed by the other line. The indirect effects of this situation are complex and can effectively increase the optical depth of a line from a population modification point of view, whilst decreasing it from an emergent flux perspective and vice versa. If blending exists then the denominator of Eq. 20 will, in principle, not cancel. Furthermore it is not clear how the p_e expression should extend into a variable density model.

Following Bhatia & Kastner (1999), we choose to formulate the problem as follows:

$$I \sim \int_{l.o.s.} N_u^{(o.thick)}(\mathbf{r}) A_{u\to l}^{(o.thin)} g\{\tau_0(\mathbf{x},\mathbf{r})\} dl \qquad (21)$$

where $N_u^{(o.thick)}(\mathbf{r})$ is obtained via the solution of Eq. 6.

The use of absorption factors, or indeed escape factors, in the statistical balance equations to calculate an optically thick population structure has been considered by a number of authors (eg. McWhirter 1965; Kastner & Bhatia 1989; Bhatia & Kastner 1992, 1999; Brooks et al. 2000). The escape factor – the escape probability averaged over every line of sight through the layer – is often used in this context as it was shown by Irons (1979) that this quantity is equivalent to the absorption factor averaged throughout the layer. Bhatia & Kastner (1999) calculated optically thick populations iteratively starting from an optically thin solution and assuming that the source function (j_ν/κ_ν) is constant throughout the emitting layer. Here we take a similar approach but for each iteration the populations are calculated at every point throughout the layer using the resolved absorption factor – the absorption factor as a function of space – to obtain an optically thick upper level population distribution (see Fig. 1). Thus here the spatial variation of the source function is included within the iterative process.

If we assume a stratified atmosphere where N_l and N_u are purely functions of height, h, above the solar surface then the absorption factor may be written as

$$\Lambda(h) \;=\; 1 - \frac{N_l(h)}{N_u(h)} \frac{\kappa_0}{2\sqrt{\pi}} \int_{-\infty}^{\infty} e^{-2u^2} \times \int_0^{\Delta x} N_u(x) E_1\left\{\tau_0(h,x) e^{-u^2}\right\} dx du \qquad (22)$$

where E_1 is the first exponential integral.

From the lower level models described below, absorption factors were calculated throughout the layer. These were calculated iteratively assuming an initial optically thin solution since the evaluation of Λ requires knowledge of the upper level population distribution. The results of this calculation are illustrated in Fig. 1 for model 3 (see below) which comprises of a layer with a density which varies exponentially with height above the solar surface.

Interestingly, upon iteration the optically thick upper level distributions of the levels of interest here (see Fig. 1b) tend to $const \times N_l(h)$. This adds weight to the assumption that

$$\frac{N_u(\mathbf{r})}{N_l(\mathbf{r})} = const \quad \text{for all} \quad \mathbf{r} \qquad (23)$$

If this assumption is made then Eq. 21 reduces to Eq. 13 as follows:

$$I = \frac{1}{4\pi} A_{u\to l} \int_0^{\Delta x} N_u(x) g\left\{-\tilde{\kappa}_0 \int_0^x N_l(x') dx'\right\} dx \qquad (24)$$

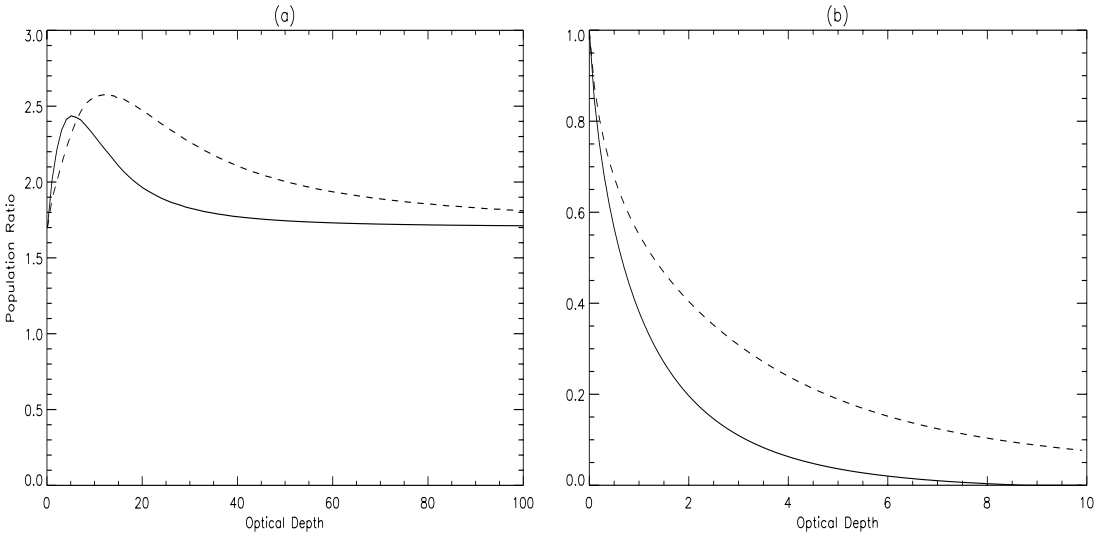

Fig. 2. **a** The population density ratio of C III ($2p^2\ ^3P_2$)/($2p^2\ ^3P_1$) vs optical depth including blending, calculated using Eq. 31 (solid line), compared with the unblended calculation based on Eq. 28 (dashed line). Photons emitted in the 2–2 line may be absorbed by the 1–1 line and vice versa effectively increasing the optical depths in each line. Consequently the blended curve varies as the unblended one with a scaled optical depth. However, absorption of 2–2 photons by the 1–1 line enhances the $2p^2\ ^3P_1$ level, lowering the population ratio. **b** $\bar{g}$ unblended (dashed) and $\bar{\bar{g}}$ blended (solid) vs optical depth. Since the optical depth ratio of the (1-2) line to the (2-1) line is ~ 1, their photon flux ratio is largely independent of the ratio of their $\bar{g}$'s and thus is proportional to the curve in **a**. Photon flux ratios that do not have comparable optical depths and do not share a common upper level vary with optical depth in a manner that displays characteristics of both the curve in **a** and that in Fig. 8. Such behaviour is evident in Fig. 3 of Bhatia & Kastner (1999).

If we define $\bar{N}_l$ as

$$\bar{N}_l = \frac{\int_0^{\Delta x} N_l(x')dx'}{\Delta x} \tag{25}$$

and make the substitution

$$s = \frac{\int_0^{x} N_l(x')dx'}{\bar{N}_l} \tag{26}$$

then Eq. 24 becomes

$$\begin{aligned} I &= \frac{1}{4\pi} A_{u\to l} \int_0^{\Delta x} \bar{N}_u g\{-\tilde{\kappa}_0 \bar{N}_l s\} ds \\ &= \frac{1}{4\pi} A_{u\to l} \bar{N}_u \bar{g}\{\tau_0\} \Delta x \end{aligned} \tag{27}$$

A similar argument shows that in making the assumption of Eq. 23, $\Lambda(h)$ reduces to $\bar{\bar{g}}\{\tau_0\}$ where

$$\begin{aligned} \bar{\bar{g}}\{\tau_0\} &= 1 - \frac{1}{\sqrt{\pi}} \int_{-\infty}^{\infty} \Big[exp\big\{ -\tau_0 e^{-u^2}/2 \big\} \\ &\quad + \big(\tau_0 e^{-u^2}/2\big) \times E_1\big(\tau_0 e^{-u^2}/2\big) \Big] e^{-u^2} du \end{aligned} \tag{28}$$

This quantity was derived in paper I.

2.3. Line blending

As discussed in Sect. 2.2, the overlap of spectral lines in frequency space influences both the emergent intensities and the population structure. Emitted photons may be absorbed by any line whose absorption profile overlaps at the nominal frequency. Furthermore the intensity term, $\bar{I}_\nu$, in Eq. 6 refers to the total intensity at frequency ν, not just that resulting from the line in question.

Blending may be included trivially within the expressions for g, $\bar{g}$, $\bar{\bar{g}}$ and Λ. The results for $\bar{g}$ and $\bar{\bar{g}}$ are shown below for line *i*.

$$\bar{g}^{(i)} = \frac{1}{\sqrt{\pi}} \int_{-\infty}^{\infty} e^{-u^2} \left\{ \frac{1 - exp[-\sum\limits_n \tau_0^{(n)} e^{-(u+v_{in})^2}]}{\sum\limits_n \tau_0^{(n)} e^{-(u+v_{in})^2}} \right\} du \tag{29}$$

where

$$v_{in} = \frac{\nu_0^{(i)} - \nu_0^{(n)}}{\Delta\nu} \tag{30}$$

$$\begin{aligned} \bar{\bar{g}}^{(i)} &= 1 - \frac{1}{\sqrt{\pi}} \frac{\omega_u^{(i)}}{\omega_l^{(i)}} \\ &\quad \times \int_{-\infty}^{\infty} e^{-u^2} \frac{\sum\limits_n \frac{\omega_l^{(n)}}{\omega_u^{(n)}} \frac{N_u^{(n)}}{N_u^{(i)}} \frac{\tilde{\kappa}_0^{(n)}}{\tilde{\kappa}_0^{(i)}} e^{-(u+v_{in})^2}}{\sum\limits_n \frac{\tau_0^{(n)}}{\tau_0^{(i)}} e^{-(u+v_{in})^2}} \\ &\quad \times \Bigg[1 - exp\big\{ -\sum_n \tau_0^{(n)} e^{-(u+v_{in})^2}/2 \big\} \\ &\qquad + \big(\sum_n \tau_0^{(n)} e^{-(u+v_{in})^2}/2 \big) \\ &\qquad \times E_1\big(\sum_n \tau_0^{(n)} e^{-(u+v_{in})^2}/2 \big) \Bigg] du \end{aligned} \tag{31}$$

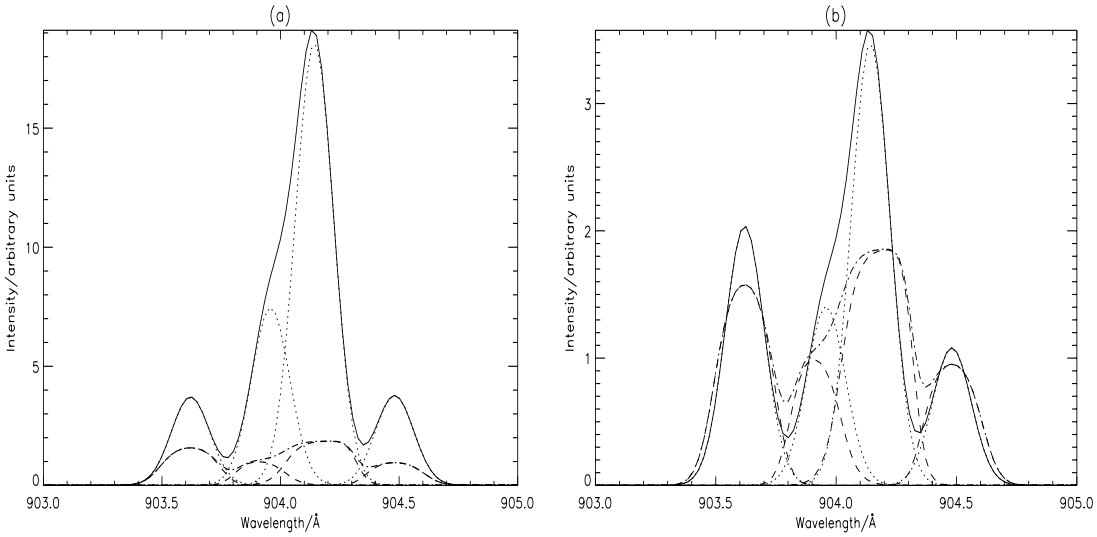

Fig. 3. **a** The C II $2s^2 2p\ ^2P$ – $2s2p^2\ ^2S$ multiplet for the optically thin case (dotted and solid lines) and the case where the optical depth of the (3/2-3/2) component at 904.143 Å is 10 (dashed and chain lines) calculated using Eqs. 29 and 31. **b** The dotted and solid lines correspond to the optically thick multiplet calculated using Eqs. 14 and 28. The dashed and chain lines are as in **a**.

Fig. 3a shows the C II $2s^2 2p\ ^2P$ – $2s2p^2\ ^2P$ multiplet for the case where the optical depth of the 3/2–1/2 component at 904.143 Å is 10, calculated using Eqs. 29 and 31, in comparison with the optically thin case. Fig. 3b shows the same in comparison with the thick multiplet calculated using Eqs. 14 and 28. These show that there is a clear difference in both intensity and line shape when blending is included. Note that the multiplet components are labelled by their J quantum numbers.

3. Atmosphere models and scattered light

We wish to combine the simple escape probability and absorption factor techniques with atmosphere models to predict both the emergent spectral line fluxes and flux ratios. Spectral emission from quiet sun regions of the upper chromosphere and transition zone is dominated by spicule-like inhomogeneities and so one would expect any successful model to account for these features.

We consider four models: firstly we consider emission following the $G(T_e)$ function[1] with a transition-zone layer based on constant conductive flux from the corona to the chromosphere. T_e and N_e follow the quiet sun atmosphere model of Vernazza et al. (1981). Secondly, following the approach of Kastner & Bhatia (1992), an emission layer of constant (adjustable) thickness and density is envisaged. This model is a simple parametric adjustment which does not attempt to capture anything of the nature of the spicules. It is, nevertheless, useful to consider such a model in order to put the success of any other simple model in context. Thirdly, a layer of density which falls off exponentially with adjustable scale height is envisaged. That is, the density falls off as $Be^{-x/H}$ for some constants H and B. This is motivated by the findings of Mariska et al. (1978) who considered models where the dominant contribution to the EUV signal was due to transition-zone sheaths around isolated cylindrical Hα spicules but showed that 'above the emission peak the amount of emitting material in the line of sight for any spectral line must decrease exponentially with height with a scale height that depends on temperature'. Furthermore this is identical, in essence if not approach, to the model of Withbroe & Mariska (1976). Finally we consider a composite of models 1 and 3, i.e. a thin layer plus a layer of exponentially decaying density of adjustable scale height. The relative magnitude of the thin layer to the other is adjusted to optimise the fit to the data but the quality of the fit is insensitive to this parameter.

In summary the models considered are

1. Thin transition region based on the VAL atmosphere model
2. Spherical shell of constant density
3. Layer of density that falls off exponentially with height
4. Composite of models 1 and 3

3.1. Scattered light

In all four models it was necessary to consider the effects of instrumentally scattered light - light that reflects off the interior of the telescope prior to passing through the entrance slit. The entire disk contributes to the scattered light signal with the contribution from each point being characterised by the instrument point spread function, *psf*, (Fig. 4) – the relative intensity of a point source as a function of lateral distance from the slit. David et al. (1997) have shown that the pre-launch point spread function is still effective so it was this that was used to complete the calculation. Thus the emitted flux, $\mathcal{F}$, from position $\mathbf{h}$ is given by

$$\mathcal{F}(\mathbf{h}) = \int\int_{disk} \mathcal{F}_t(\mathbf{x}) \times psf(|\mathbf{h}-\mathbf{x}|)d\mathbf{x} \qquad (32)$$

[1] The $G(T_e)$ function describes the emission from a particular transition as a function of electron temperature.

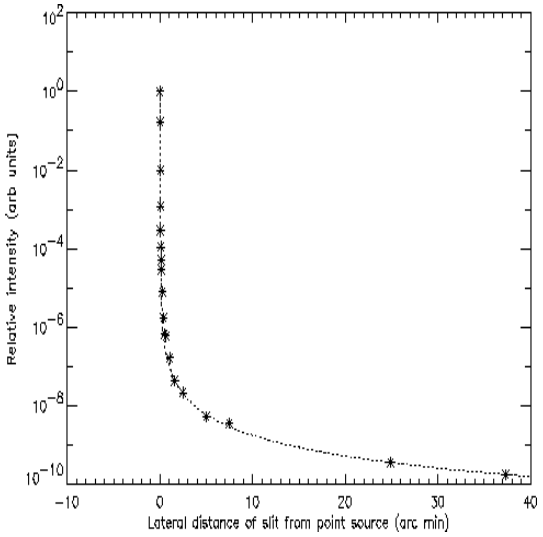

Fig. 4. The SUMER pre-launch point spread function (stars) (Lemaire 1998) – relative intensity of a point source vs lateral distance from source to slit centre. The dotted line is a fit to the measured points used in the analysis described.

where $\mathcal{F}_t(\mathbf{x})$ is the true signal $= const \times \bar{I}(\mathbf{x})$.

In practice we have evaluated this integral along a radius rather than over the whole disk. This introduces an error in that the scattered contribution is underestimated at each point by a maximum factor of 2π but this error is not sufficient to explain the C III emission beyond $\sim$ 970 arc sec. The calculation captures well the dependance of the off-limb line ratios on scattered light.

4. Model predictions

In September 1996 a SUMER observing sequence called OPAC was run which consisted of around 20 west-east scans of the east solar limb. Each scan involved 18 steps using the 1x120 arc sec slit. The C II and C III data used in the analysis described below are from this sequence. The theoretical atomic data used for the modelling of C II and C III populations follow from paper I and are drawn from the Atomic Data and Analysis Structure (ADAS, see Summers 1993, 1999).

4.1. Fluxes

The observed spectral line fluxes for the C II $2s^2 2p\ ^2P_{3/2} - 2s2p^2\ ^2S_{1/2}$ line at 1037.020 Å and the C III $2s2p\ ^3P_2 - 2p^2\ ^3P_2$ line at 1175.711 Å are shown in Fig. 5a and b respectively with the predicted fluxes (calculated via Eq. 27) overlayed. Model 1 fails completely for both C II and C III as expected as it does not recognise the extension of the transition region into the corona due to spicules and other structures. Models 2, 3 and 4 track the trend in both cases in broad terms but not in detail, failing most markedly at the limb and well off limb. On disk despite the averaging over the slit, the fluxes display a sensitivity to structure which is evident in the surface plots of Fig. 6. This sensitivity to column density is implied by Eq. 27 since $\bar{g}$ is insensitive to optical depth for optical depths greater than $\sim$ 1.

At heights of $\sim$ 970 arc sec and above the observed signal is orders of magnitude greater than that predicted. Since the scattered light calculations are expected to be in error by a maximum factor of $\sim 2\pi$ this signal is possibly of solar origin. If this is so then the fact that the ratios at these heights indicate optical depths similar to that on disk, implies that the emitting structures here must be unresolved.

4.2. Ratios

The observed and model flux ratios of the (3/2–1/2)/(1/2–1/2) components of the C II $2s^2 2p\ ^2P - 2s2p^2\ ^2S$ multiplet and the (2–2)/(1–1) components of the C III $2s2p\ ^3P - 2p^2\ ^3P$ multiplet are shown in Fig. 7a and b respectively. The models here are much more effective since the linear dependence on column density is factored out (see Eq. 15). In the C III case the dip in the ratios at the limb is underestimated yet optical depths at this point are such that the $\bar{g}$ ratio, in the absence of blending, is insensitive to optical depth. When blending is included, absorption of 2–2 line photons by the 1–1 line leads to a decrease in the ratio. The underestimation of the ratios at the limb suggests an underestimate in lower level population density of either the 2–2 line or the 1–1 line yet at this point the emergent intensities are overestimated suggesting an overestimate in the upper level column densities. This discrepancy is possibly due to a dependence of the absorption factor on homogeneity. The general insensitivity of the ratios themselves, and the relative success of the stratified model in predicting them suggests, however, that this dependence is weak. This is further supported by the insensitivity of $\bar{\bar{g}}$ to optical depth for optical depths greater than $\sim$ 1 (see Fig. 2b).

5. Discussion

The best fit to the observed ratios for each model yielded optimal parameters for each model and for each of the two ions. The two most effective models in each case were models 3 and 4 for which the most significant parameter is the density scale height. Optimisation of this parameter yields scale heights of 1.2 and 2.5 arc sec for both models 3 and 4 for C II and C III respectively. Fig. 7b shows that within the pointing accuracy of the SUMER instrument (around 10 arc sec – see paper I), model 4 is slightly more effective than model 3 in describing the C III ratio variation across the limb. However, the relative magnitude of model 1 to model 3 in the composite case was treated as an adjustable parameter and whilst a large value ($\sim$ 100) is optimal in the C III case, a low value, namely zero, is the optimal value for C II. As a consequence it is felt that model 4 is, in this study, largely redundant. The scale heights in both cases are similar to the $\sim$ 1.5 arc sec findings of Mariska, Feldman & Doschek and to those found in paper I – noting that the C III scale height is likely to be an over estimate as the slope of the ratios in the region from 964 $\rightarrow$ 970 arc sec is not matched. They also agree

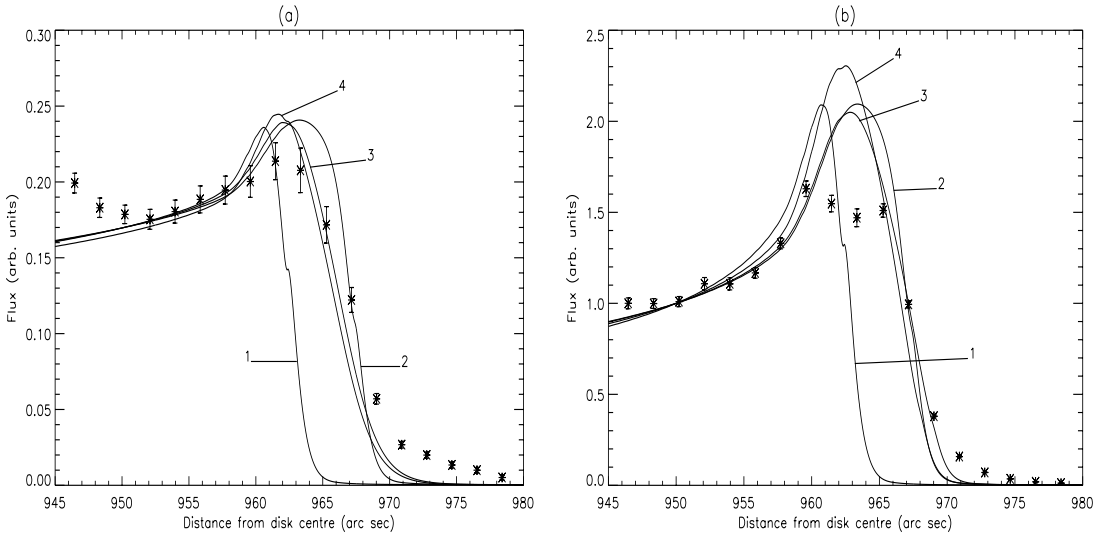

Fig. 5a and b. Observed and model fluxes for the **a** C II $2s^2 2p\ ^2P_{3/2} - 2s2p^2\ ^2S_{1/2}$ line at 1037.020 Å and **b** the C III $2s2p\ ^3P_2 - 2p^2\ ^3P_2$ line at 1175.711 Å. The stars correspond to the observed fluxes and the solid lines are the model predictions numbered as above. Note that the visible limb is at 959.6 arc sec.

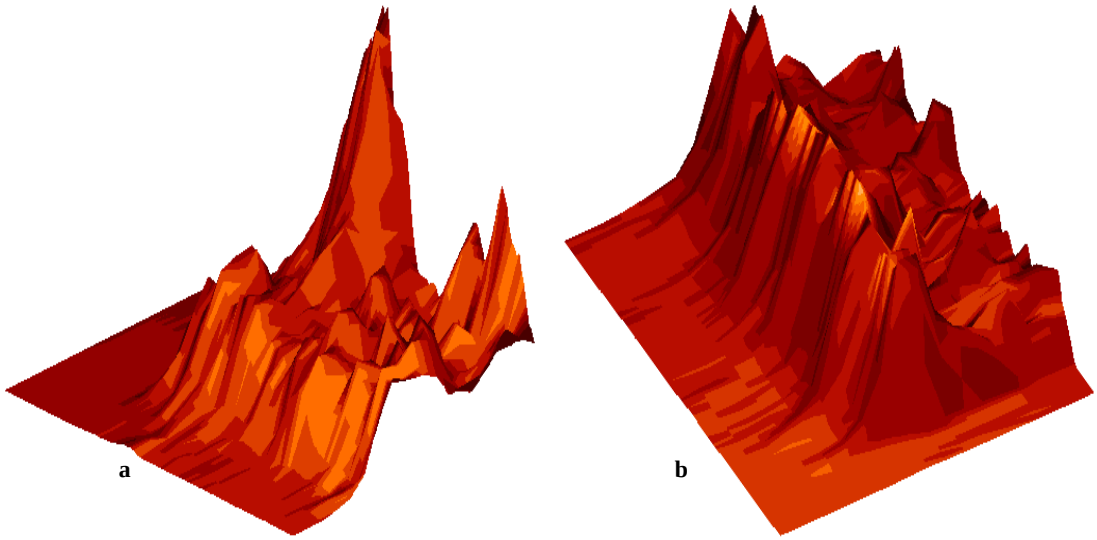

Fig. 6a and b. Surface plots of the **a** C II $2s^2 2p\ ^2P - 2s2p^2\ ^2P$ and **b** C III $2s2p\ ^3P - 2p^2\ ^3P$ multiplets at $\sim$ 904 Å and 1175 Å respectively, showing total flux in the slit/raster plane. The slit dimension runs from bottom right to top left and the raster dimension runs from top right to bottom left.

with both in terms of the decrease with decreasing temperature of line formation.

In order for the scattered light to dominate at the appropriate points, a departure from the exponential fall off of density is required. A cut-off was introduced in the model for this purpose, the position of which was optimised for agreement with the observed ratios. For C II the optimal position was found to be $\sim$ 974 arc sec. For C III this cut-off was found to be at $\sim$ 969 arc sec. This latter value is influenced by the fact that the scale height is optimised as described above and is thus overestimated. Consequently in the absence of a cut-off the predicted onset of scattered light occurs later than observed.

A possible interpretation for this departure from an exponential fall off, or at least a change or even discontinuity in scale height, follows from the model considered by Mariska, Feldman & Doschek who, as stated above, envisaged cylindrical spicules. The exponential fall off of density in this picture reflects the change in filling factor as the number of spicules intersected by the line of sight decreases with distance beyond the limb. Ultimately, however, the density variation will reflect the genuine density variation at the top of a spicule.

In paper I the extension of the line of sight with raster position was treated as a single effect on the layer as a whole for each density model. However, in the variable density case, lines of sight at and near the limb see a greater geometric extension of the line of sight for the inner most sublayers compared to those toward the outer extreme of the emitting layer. Since these inner sublayers correspond to regions of higher density, a

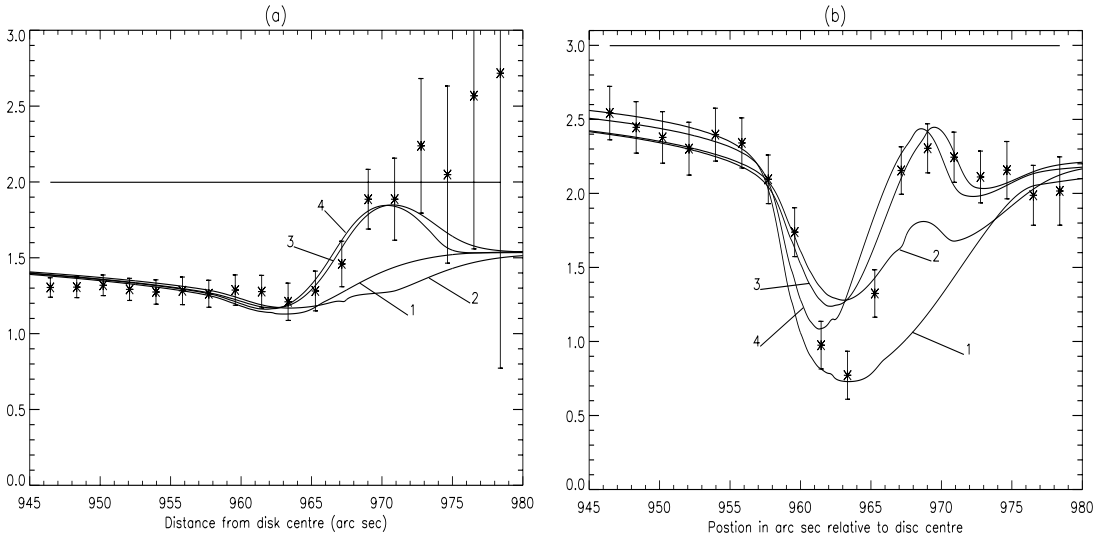

Fig. 7a and b. Observed and model flux ratios of the **a** (3/2–1/2)/(1/2–1/2) components of the C II $2s^2 2p\ ^2P$ – $2s2p^2\ ^2S$ multiplet and **b** the (2–2)/(1–2) components of the C III $2s2p\ ^3P$ – $2p^2\ ^3P$ multiplet. Note that in **a** the results of models 3 and 4 are almost identical.

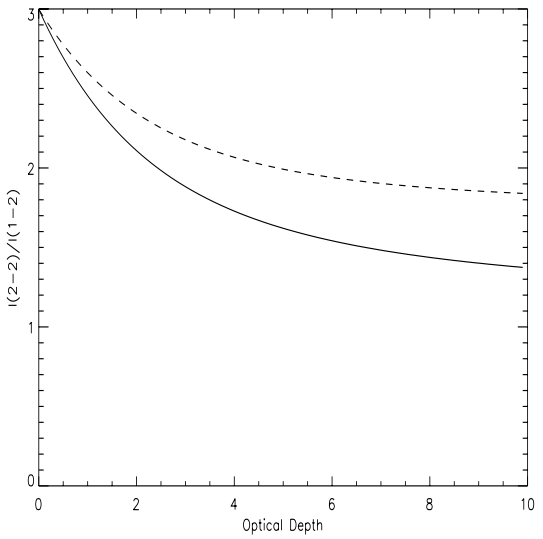

Fig. 8. Intensity ratio of C III (2–2)/(1–2) vs optical depth for the unblended (dashed) and blended (solid) cases.

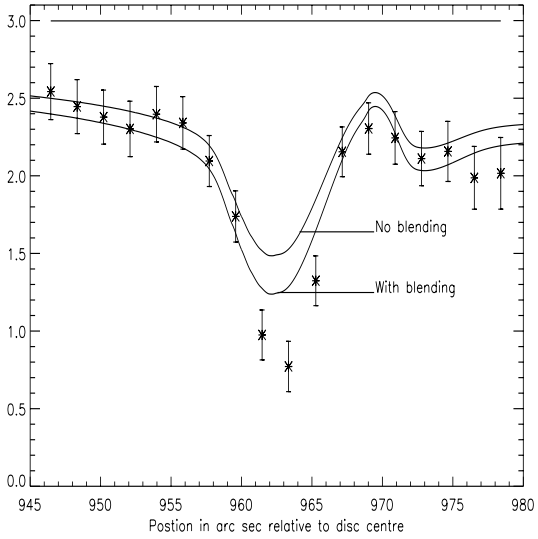

Fig. 9. Observed and model flux ratios of the (2–2)/(1–2) lines of the C III $2s2p\ ^3P$ – $2p^2\ ^3P$ multiplet for model 3 in the blended and unblended case.

proper treatment of the geometric extension leads to a greater variation of optical depth between the disk and the limb (and hence a stronger dip in the C III ratios at the limb) in comparison with a model that only considers the geometric extension of the emitting layer as a whole. With this in mind it is interesting to note the comparative success of the simpler escape probability approach of paper I and of Doyle & McWhirter (1981) in regard to the ratio behaviour of C III in the vicinity of the limb. In both these works the line of sight extension was modelled as $const/cos\theta$ where θ is 0 at disc centre and $\pi/2$ at the limb. This is infinite at the layer edge (hence the discontinuity in the models in Figs. 13, 14 and 15 of paper I at this point) and consequently the extension of the line of sight is overestimated as are the optical depths in this region. This error serves to improve the fit to the data.

6. Conclusions

The escape probability approach in conjunction with a simple stratified atmosphere model is effective in describing the limb brightening and ratio variation curves of the C II and C III data considered here. The most effective model is found to be a layer of density that varies exponentially with height, agreeing qualitatively with the findings of Mariska et al. (1978). Optimal density scale heights were found to be 1.2 arc sec for C II and 2.5 arc sec for C III although the result for C III is felt to be an overestimation given the models' underestimate of the extent of the dip in the ratios upon crossing the limb. Cutoffs were included to ensure the onset of scattered light dominance at 974 and 969 arc sec for C II and C III respectively. A physical inter-

pretation of this is that the exponential fall off of density reflects the reduction of the number of spicules intersected by the line of sight whereas the cutoff represents the actual fall off of density at the top of a spicule. The fact that the cutoff is greater for the lower temperature emission is possibly due to the overestimate of the C III scale height. However, it could be linked with the apparent evidence in the observed fluxes of unresolved optically thick structures extending to greater heights.

The escape probability approach has been further simplified since the optical depths relevant here are moderate. Thus the population modification leads to negligible distortion of the upper level population distribution relative to the lower level distribution and so it may be assumed that they differ by a constant. This assumption allows the layer averaged escape probability, $\bar{g}\{\tau_0\}$, to be used.

Due to the approximately linear dependence of intensity on upper level column density, even the average limb brightening curves display a sensitivity to atmospheric structure. In contrast, the ratios reflect more the dependence of the escape probability on optical depth and are thus less sensitive. This suggests that, since $\bar{\bar{g}}$ is similarly insensitive to optical depth for optical depths greater than ~ 1, and, as Eq. 6 shows, the general quantity Λ is a function of the radiation field – a quantity that represents an integral over space and thus a degree of averaging over inhomogeneity – the population modification itself is relatively insensitive to inhomogeneity.

A principle motivation for this work was to assess the potential of the simple escape probability techniques for use within dynamic atmosphere models. In a fully resolved picture the dynamic evaluation of Λ point to point is arduous. However, the insensitivity to structure suggests that the absorption factors may be well approximated using a stratified (averaged) atmosphere model, or even using $\bar{\bar{g}}$. Since the emergent intensities are more sensitive to structure the fully resolved model must be used in Eqs. 12 or 27 (whichever is appropriate). This may be done with no increase in computational effort.

Line blending, when significant, has a marked influence on both the emergent intensities and the population structure. Blending may be easily included within all the escape probability and absorption factor expressions.

Acknowledgements. We wish to thank D. Brooks for his valuable input. GF acknowledges an EPSRC studentship and SL acknowledges an EPSRC-CASE studentship with the Rutherford Appleton Laboratory. SOHO is a project of international co-operation between ESA and NASA.

References

Bhatia A.K., Kastner S.O., 1992, ApJS 79, 139
Bhatia A.K., Kastner S.O., 1999, ApJ 516, 482
Brooks D.H., Fischbacher G.A., Fludra A., et al., 2000, A&A in press
David C., Gabriel A.H., Bely-Debau, 1997, Proceedings of the Fifth SOHO Workshop, Oslo, Norway, 17-20 June, 1997
Doyle J.G., McWhirter R.W.P., 1980, MNRAS 193, 947
Doschek G.A., et al., 1976, ApJ 31, 417
Holstein T., 1947, Phys. Rev. 72, 1212
Irons F.E., 1979, J. Quant. Spectrosc. Rad. Trans. 22, 1
Jordan C., 1967, Solar Physics 2, 441
Kastner S.O., Bhatia A.K., 1989, ApJS 71, 665
Kastner S.O., Bhatia A.K., 1992, ApJ 401, 416
Kastner S.O., Kastner Ruth E., 1990, J. Quant. Spectrosc. Rad. Trans. 44, No. 2, 275
Lemaire P., 1998, private communication
Mariska J.T., Feldman U., Doschek G.A., 1978, ApJ 226, 698
McWhirter R.W.P., 1965, In: Huddlestone R.H., Leonard D.H. (eds.) Plasma Diagnostic Techniques
Summers H.P., 1993, JET Joint Undertaking Report, JET-IR(93)07
Summers H.P., 1999, The ADAS User Manual. version 2.1, http://patiala.phys.strath.ac.uk/adas/
Vernazza J.E., Avrett E.H., Loeser R., 1981, ApJS 45, 635
Withbroe G.L., Mariska J.T., 1976, Solar Physics 48, 21